ACS APPLIED MATERIALS & INTERFACES

Research Article

www.acsami.org

On the Utility of Spinel Oxide Hosts for Magnesium-Ion Batteries

James C. Knight,[†] Soosairaj Therese,[‡,§] and Arumugam Manthiram*[,†,‡]

[†]McKetta Department of Chemical Engineering, University of Texas at Austin, Austin, Texas 78712, United States

[‡]Materials Science and Engineering Program, University of Texas at Austin, Austin, Texas 78712, United States

[§]Department of Chemistry and Chemical Technology, Bronx Community College, Bronx, New York 10453, United States

Supporting Information

ABSTRACT: There is immense interest to develop Mg-ion batteries, but finding suitable cathode materials has been a challenge. The spinel structure has many advantages for ion insertion and has been successfully used in Li-ion batteries. We present here findings on the attempts to extract Mg from $MgMn_2O_4$-based spinels with acid (H_2SO_4) and with NO_2BF_4. The acid treatment was able to fully remove all Mg from $MgMn_2O_4$ by following a mechanism involving the disproportionation of Mn^{3+}, and the extraction rate decreased with increasing cation disorder. Samples with additional Mg^{2+} ions in the octahedral sites (e.g., $Mg_{1.1}Mn_{1.9}O_4$ and $Mg_{1.5}Mn_{1.5}O_4$) also exhibit complete or near complete demagnesiation due to an additional mechanism involving ion exchange of Mg^{2+} by H^+, but no Mg could be extracted from $MgMnAlO_4$ due to the disruption of Mn−Mn interaction/contact across shared octahedral edges. In contrast, no Mg could be extracted with the oxidizing agent NO_2BF_4 from $MgMn_2O_4$ or $Mg_{1.5}Mn_{1.5}O_4$ as the electrostatic repulsion between the divalent Mg^{2+} ions prevents Mg^{2+} diffusion through the 16c octahedral sites, unlike Li^+ diffusion, suggesting that spinels may not serve as potential hosts for Mg-ion batteries. The ability to extract Mg with acid in contrast to that with NO_2BF_4 is attributed to Mn dissolution from the lattice and the consequent reduction in electrostatic repulsion. The findings could provide insights toward the design of Mg hosts for Mg-ion batteries.

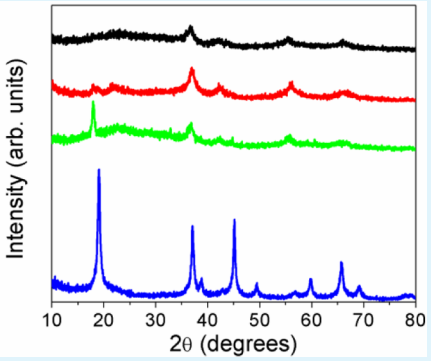

KEYWORDS: *Mg spinels, Mg-ion batteries, Mg extraction, acid extraction, chemical extraction*

1. INTRODUCTION

Li-ion batteries have become increasingly prevalent in modern society as they power personal electronic devices and automobiles due to their high energy density.[1] There are several issues, however, with Li-ion batteries, such as safety concerns, high cost, and limited charge-storage capacity.[1] With an aim to increase the capacity, much attention is focused toward multivalent cation systems (Mg^{2+}, Al^{3+}, etc.) because of their ability to hold greater amounts of charge.[2,3] Mg-ion batteries also offer additional advantages such as reduced cost and better safety with Mg-metal anodes.[4] However, Mg-ion batteries pose numerous challenges such as incompatibility of the Mg-metal anode with nonaqueous electrolytes due to the formation of a passivating layer that blocks Mg-ion diffusion, poor kinetics of Mg^{2+}-ion diffusion, lack of electrolytes with wide stability windows, and lack of cathode hosts with high operating voltages.[4]

Significant efforts are being put into finding suitable cathodes for Mg-ion batteries, but it is challenging due to the 2+ charge on Mg^{2+} ions, which leads to strong interactions with the host structure ions that limit the Mg diffusion kinetics.[5] This leads to the failure of most metal oxide hosts analogous to lithium-ion cathodes as Mg insertion hosts. The most successful cathodes to date are Chevrel-phase compounds based on Mo_6S_8, are able to accommodate the electrons within the Mo_6 clusters.[6] However, despite good cyclability, the Chevrel phase is not promising for commercial applications because of their low operating voltage and capacity.[7−10] Various MnO_2 polymorphs, including α-, stabilized α-, β-, γ-, and δ-MnO_2, have also been explored with varying degrees of effectiveness.[11−13] The most successful polymorphs were α-MnO_2 nanorods with high surface areas and δ-MnO_2 (birnessite). Mg^{2+} insertion into the birnessite structure is made possible by the charge screening effect of the crystal water molecules present between MnO_6 layers. Other materials that have inserted Mg to various extents include V_2O_5,[5,14] MoO_3,[15] olivine silicates,[16,17] and fluorinated graphite,[18,19] among others.[20−25] Theoretical calculations have suggested that the postspinel structure, which is a denser polymorph of the spinel structure formed under high pressure with distorted MO_6 octahedra, may be a suitable host, but this has not been experimentally confirmed.[26]

The spinels are another family of materials being studied as potential cathodes because of their success in Li-ion batteries, fast ion diffusion derived from its three-dimensional ion mobility, high operating voltage, and structural stability.[1] Spinels have the chemical formula AB_2O_4, where the oxide ions form a cubic-close-packed structure. The A ions reside in 8a tetrahedral sites, and the B ions reside in alternating

Received: July 9, 2015
Accepted: October 5, 2015
Published: October 5, 2015

DOI: 10.1021/acsami.5b06179
ACS Appl. Mater. Interfaces 2015, 7, 22953−22961

octahedral sites along the three crystallographic axes, designated as 16d sites. The remaining empty octahedral sites are designated as 16c sites. In fact, several researchers claim to have used spinel-structured Mn_2O_4 (λ-MnO_2) to intercalate Mg^{2+} ions in aqueous environments.[27,28] Kim et al. recently verified the intercalation of Mg ions into λ-MnO_2 through the use of high-resolution imaging, spectroscopic measurements, and structural diffraction analysis.[29] They found that Mg^{2+} ions could be reversibly inserted into the spinel structure and that water molecules most likely do not accompany the Mg ions into the structure due to the size of the solvated ion.

Because of the success of spinel $LiMn_2O_4$ as a Li-ion battery cathode, an investigation of the mechanism of Mg extraction from $MgMn_2O_4$ and other Mg spinels could provide important insights into their applicability as Mg-ion battery cathodes. With this perspective, we employ two different chemical methods to attempt to extract Mg from $Mg_{1+x}Mn_{2-x}O_4$ (x = 0, 0.1, and 0.5) and $MgMnAlO_4$. The first method uses dilute H_2SO_4 medium to extract Mg. Hunter used this method previously to remove Li from $LiMn_2O_4$, involving the disproportionation of Mn^{3+} ions into Mn^{4+} and Mn^{2+} and resulting in the formation of λ-MnO_2 maintaining the Mn_2O_4 spinel framework.[30] The mechanism is shown below in Reaction 1:

$$LiMn_2^{3.5+}O_4 \rightarrow 0.75Mn_2^{4+}O_4 + 0.5MnO + 0.5Li_2O \quad (1)$$

The MnO and Li_2O are soluble in the acidic medium used, so only the Mn_2O_4 powder is left. Technically, $Mn_{1.5}O_3$ is the composition of the remaining solid, but it has been normalized to indicate that it still has the spinel structure.

We have previously used this method to examine the delithiation mechanism of doped $LiMn_2O_4$ and demonstrated that the amount of delithiation is dependent on the amount of Mn^{3+} ions present in the structure.[31] This will be referred to as acid demagnesiation in this study. The second method will be referred to as chemical demagnesiation in this study, and it involves stirring the samples in an acetonitrile solution containing the oxidizer nitronium tetrafluoroborate (NO_2BF_4). This reaction mechanism is controlled by the amount of NO_2BF_4 used, as opposed to the acid treatment, which depends on the material composition, viz., Mn^{3+} content. The ability to extract Mg^{2+} oxidatively with the oxidizing agent NO_2BF_4 can shed light on whether or not spinels can serve as potential hosts for Mg-ion batteries.

2. EXPERIMENTAL SECTION

2.1. Synthesis. All the samples were synthesized with a sol−gel method, and a representative description is given here. Required amounts of Mg acetate, Mn acetate, and Al nitrate were dissolved in 100 mL of stirring deionized (DI) water. The total amount of metal ions was 0.025 mol in each reaction. Citric acid was then dissolved in the solution, with a 1:1 mol ratio of metal ions to citric acid. The solution was stirred and heated on a hot plate until all of the liquid evaporated. The resulting material was calcined in a furnace to 450 °C for 5 h with heating and cooling rates of 3 °C/min. The powder obtained was then pelletized and heated at a designated temperature for 12 h with a heating rate of 3 °C/min, followed by quenching into liquid nitrogen. $MgMn_2O_4$, $Mg_{1.1}Mn_{1.9}O_4$, and $MgMnAlO_4$ were calcined at 1000 °C, while $Mg_{1.5}Mn_{1.5}O_4$ was calcined at 850 °C. An additional $MgMn_2O_4$ sample was calcined at 1200 °C. After this high temperature heat treatment, some samples were annealed at 400 °C for 12 h with heating and cooling rates of 3 °C/min.

2.2. Demagnesiation and Characterization. Two different methods were utilized to extract magnesium from the lattice. The acid demagnesiation involved the addition of 0.25 g of active material to 25 mL of 0.35 N H_2SO_4 and stirring in a flask for 24 h. The product was then recovered by filtration and dried at 100 °C overnight. The chemical demagnesiation involved placing 0.25 g of active material in a flask inside an Ar-filled glovebox, followed by the addition of 1 g of NO_2BF_4 and capping the flask. Then, 10 mL of anhydrous acetonitrile was added into the capped flask and stirred for 24 h under Ar with a Schlenk line. The product formed was recovered after filtration with acetonitrile and acetone and drying overnight at 100 °C.

The samples were characterized before and after the treatment with acid or NO_2BF_4 by X-ray diffraction (XRD) and inductively coupled plasma (ICP) analysis. A Varian 715-ES was used for ICP analysis. The ICP values had an error bar of ±0.02, and the percent relative standard deviations (% RSDs) for each measurement were under 3%. XRD analysis was carried out with a Rigaku Miniflex 600 with Cu Kα radiation at 10−80° with a step size of 0.02° and a scan rate of 2°/min. Cation disorder values for the $MgMn_2O_4$ samples were obtained by the Rietveld refinement method using the General Structure Analysis Software (GSAS, Los Alamos National Laboratory) program. The tetragonal spinel structure ($I4_1/amd$) was used for the refinement for all the samples, allowing both the Mg and the Mn ions to reside in the tetrahedral and octahedral sites. Fourier transform infrared spectroscopy (FTIR) analysis was carried out with pelletized KBr samples employing a Thermo Fisher Scientific Nicolet iS5 instrument.

3. RESULTS AND DISCUSSION

3.1. Acid Treatment of $MgMn_2O_4$. The first compound studied was $MgMn_2O_4$, which is structurally similar to spinel $LiMn_2O_4$. The Mg ions reside in the 8a tetrahedral sites like Li, and the Mn ions reside in the 16d octahedral sites. However, there are some key differences between the two materials. In $LiMn_2O_4$, half of the Mn ions are in the 3+ state and half are in the 4+ state, whereas $MgMn_2O_4$ has all Mn^{3+} ions due to the higher valence of Mg. This increase in Jahn−Teller active Mn^{3+} ions causes $MgMn_2O_4$ to be a tetragonal spinel instead of the cubic spinel. Another variation between the structures is the degree of cation disorder in them. Cation disorder refers to ions supposedly in the tetrahedral sites residing in the octahedral sites and vice versa.[32] The degree of cation disorder in spinel structures is influenced by several factors, including composition, ionic size, ion valence state, octahedral site stabilization energies, calcining temperature, and cooling rate.[33−36] Because of the large size and charge differences between Li^+ and $Mn^{3+/4+}$ ions, the Li spinel possesses essentially no cation disorder. On the other hand, $MgMn_2O_4$ can experience significant cation disorder because Mg^{2+} and Mn^{3+} ions are closer in size and charge. Various degrees of cation disorder can be created by altering the heating protocol.[32,37−44] Cation disorder can also affect the oxidation state of ions in the prepared samples. For example, when a Mg^{2+} ion moves to an octahedral site, it remains a Mg^{2+} ion. However, when an Mn^{3+} ion migrates to a tetrahedral site to take the place of a Mg^{2+} ion, it is reduced to Mn^{2+} and creates a corresponding Mn^{4+} ion in an octahedral site. The average Mn oxidation state is still the same, but this can affect other properties of the material.

Four samples with different amounts of cation disorder were created, and their XRD patterns can be seen in Figure 1, as well as a reference pattern for ordered $MgMn_2O_4$. Two samples, which will be referred to as Mg 1200 and Mg 1000, were obtained by quenching, respectively, from 1200 and 1000 °C. The other two samples, which will be referred to as Mg 1200A and Mg 1000A, were obtained by annealing at 400 °C after quenching from 1200 and 1000 °C, respectively. Going from the most disordered to the least disordered, the samples are Mg 1200, Mg 1000, Mg 1200A, and Mg 1000A. A higher firing

DOI: 10.1021/acsami.5b06179
ACS Appl. Mater. Interfaces 2015, 7, 22953−22961

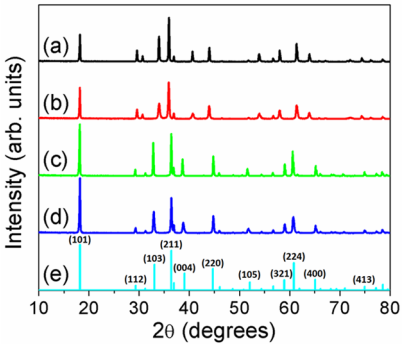

Figure 1. XRD patterns of the four $MgMn_2O_4$ starting materials with varying degrees of cation disorder: (a) Mg 1200, (b) Mg 1000, (c) Mg 1200A, and (d) Mg 1000A. A reference pattern for the ordered $MgMn_2O_4$ is given in (e).

temperature promotes disorder by imparting greater thermal energy to the ions, making them more likely to hop to energetically unfavorable sites. Quenching the samples in liquid nitrogen attempts to lock in the high temperature cation configuration at ambient temperatures. Annealing the samples at a lower temperature after quenching allows for the more thermodynamically stable cation arrangement to form. Mg 1000 and Mg 1200 produce very similar patterns, except for changes in peak intensity. The annealed samples, however, show significant shifts in peak positions, as the reduction in cation disorder alters the lattice parameters. The two annealed samples are similar to each other, just as the two quenched samples are, except for changes in peak intensity.

A qualitative method of comparing the cation disorder between samples is to look at the peak ratios of the (101) and (211) peaks.[42] The (211) peak at ~36.3° is often the most intense peak in the $MgMn_2O_4$ pattern, and it is not sensitive to changes in cation disorder. Conversely, the (101) peak at ~18.5° drastically decreases in intensity with increasing cation disorder, so an increasing ratio of the (101) to (211) peaks qualitatively shows a decrease in cation disorder. To quantify the cation disorder, however, Rietveld refinement was used. The findings can be found in Table 1, where the inversion degree refers to the fractional amount of Mg ions that migrate out of the tetrahedral sites and reside in the 16d octahedral sites. More detailed results of the Rietveld refinement process can be found in the Supporting Information. The samples are listed from the most disordered to the least disordered, with the most disordered sample Mg 1200 at the top. The Rietveld refinement data confirm the previously described ranking of cation disorder among the samples.

Table 1. Inversion Degree (Cation Disorder) in the Four $MgMn_2O_4$ Samples and the Theoretical and Experimental Mg Content after Acid Treatment of the Seven $Mg_{1+x}Mn_{2-x}O_4$ Samples

sample	inversion degree (%)	expected composition after acid treatment	Mg content after single acid treatment	actual composition after multiple acid treatments
Mg 1200	34	Mn_2O_4	0.46	$Mg_{0.06}Mn_2O_4$
Mg 1000	29	Mn_2O_4	0.31	$Mg_{0.05}Mn_2O_4$
Mg 1200A	6	Mn_2O_4	0.13	$Mg_{0.06}Mn_2O_4$
Mg 1000A	1	Mn_2O_4	0.05	$Mg_{0.05}Mn_2O_4$
Mg 1.1		$Mg_{0.36}Mn_{1.82}O_4$	0.31	$Mg_{0.02}Mn_{1.82}O_4$
Mg 1.1A		$Mg_{0.36}Mn_{1.82}O_4$	0.08	$Mg_{0.08}Mn_{1.82}O_4$
Mg 1.5		$Mg_{1.33}Mn_{1.33}O_4$	0.63	$Mg_{0.14}Mn_{1.33}O_4$

As Hunter previously showed,[30] $LiMn_2O_4$ can be fully delithiated by treating with dilute H_2SO_4 as depicted earlier in Reaction 1. Despite the change in the oxidation state of Mn, $MgMn_2O_4$ should experience full Mg extraction as well, which is illustrated in Reaction 2:

$$MgMn_2^{3+}O_4 \rightarrow 0.5Mn_2^{4+}O_4 + MnO + MgO \quad (2)$$

The MnO and MgO are again soluble, leaving behind only Mn_2O_4 (technically MnO_2). All four samples were stirred with acid for 24 h, and their XRD patterns after acid treatment are shown in Figure 2, along with a reference pattern for λ-MnO_2.

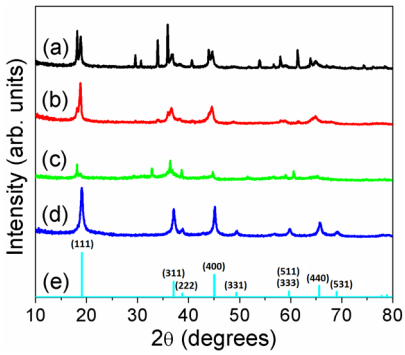

Figure 2. XRD patterns of the four $MgMn_2O_4$ samples with varying degrees of cation disorder after their first acid treatment: (a) Mg 1200, (b) Mg 1000, (c) Mg 1200A, and (d) Mg 1000A. A reference pattern for λ-MnO_2 is given in (e).

The XRD patterns for all samples, except Mg 1000A, showed several additional peaks in addition to those of the expected λ-MnO_2 pattern, signaling incomplete Mg extraction. Indeed, ICP analysis showed that the samples, except Mg 1000A, had significant amounts of Mg remaining in the structure. Those Mg content values are listed in Table 1. This is in contrast to our previous study, where all reactions were completed in this time frame.[31] Figure 2 also demonstrates the effect that cation ordering has on the structure of the acid-treated materials. Mg 1200 has almost half of the Mg remaining, so despite its high degree of cation disorder, it still has several peaks from the parent tetragonal spinel structure. Mg 1000, despite having significant Mg remaining in the structure, has relatively weak tetragonal spinel peaks remaining due to the disordered nature of the starting material. On the other hand, Mg 1200A experiences a higher degree of Mg extraction than Mg 1200 and Mg 1000, but it still produces a two-phase material with clear XRD reflections after acid treatment since the starting tetragonal spinel phase was well crystalline and ordered. Finally, Mg 1000A exhibits a single-phase λ-MnO_2 pattern after acid treatment because of the essentially complete Mg extraction and its highly ordered starting material, which allows for a more crystalline material after treatment. It should also be noted that, as the cation disorder decreases, the amount of Mg extracted increases. In other words, increasing cation order increases the rate of Mg removal. The relationship is somewhat linear, as depicted in Figure 3. Further discussion of this topic will appear in the next section.

There may be a couple of forces causing the incomplete Mg removal. The most likely cause is the increased electrostatic

DOI: 10.1021/acsami.5b06179
ACS Appl. Mater. Interfaces 2015, 7, 22953−22961

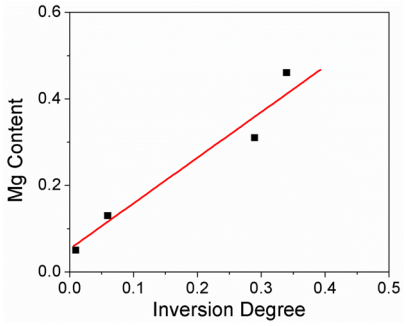

Figure 3. Plot of inversion degree (cation disorder) vs Mg content after a single acid treatment for the four $MgMn_2O_4$ samples with various heating protocols. A linear fit is also included.

repulsion felt by Mg^{2+} ions as they have a higher charge than Li^+ ions. In order to be extracted from the structure, the Mg^{2+} ions must diffuse between the 8a tetrahedral and 16c octahedral sites from the interior to the surface of the particle, so the increased repulsion between the Mg^{2+} ions in the 8a tetrahedral and 16c octahedral sites may inhibit Mg^{2+} ion diffusion through these sites. A secondary factor could be the difference in the ionic sizes and masses between Mg^{2+} and Li^+. However, Li^+ ions, with 0.59 Å in tetrahedral sites and 0.76 Å in octahedral sites, are only slightly larger than Mg^{2+} ions, with 0.57 Å in tetrahedral sites and 0.72 Å in octahedral sites, so the size difference should not affect the extraction rate much. $MgMn_2O_4$, however, has all Mn^{3+} ions (unless Mn^{4+} ions are created through cation disorder), which are larger (0.645 Å) than Mn^{4+} ions (0.53 Å). The $LiMn_2O_4$ structure has a much higher amount of the smaller Mn^{4+} ions present, possibly allowing for better ion transport. On the other hand, this size argument contradicts the finding that increased ordering leads to faster Mg removal. In a highly ordered $MgMn_2O_4$ sample, there should be almost no Mn^{4+} ions, so only the larger Mn^{3+} ions are present, which should slow down Mg removal. This, however, does not match with the experimental outcomes.

In order to see if Mg could be fully extracted from the samples, additional acid treatments were carried out after filtering and washing the samples. Mg 1000A was deemed fully converted after the first acid treatment. Mg 1200 and Mg 1000 required two additional treatments, while Mg 1200A required one more. The final Mg contents of the materials are listed in Table 1. The XRD patterns of these final materials are displayed in Figure 4 along with a λ-MnO_2 reference pattern. Clearly, increased cation ordering in the starting material led to a more crystalline phase after acid treatment. Only Mg 1000A produced a single-phase material of the expected λ-MnO_2. The other samples produced less crystalline samples with some additional peaks from other Mn oxides, Mn_3O_4, and γ-MnO_2.

3.2. Acid Treatment of $Mg_{1+x}Mn_{2-x}O_4$. Additional samples were made to test the effect of Mn oxidation state on the acid treatment mechanism. The Mn oxidation state was altered by replacing some Mn by Mg in the series $Mg_{1+x}Mn_{2-x}O_4$. As the Mg content (or x value) increases, the Mn oxidation state increases to maintain charge neutrality. The samples synthesized were $Mg_{1.1}Mn_{1.9}O_4$ (Mg 1.1) and $Mg_{1.5}Mn_{1.5}O_4$ (Mg 1.5), which have average Mn oxidation states of 3.05+ and 3.33+, respectively. Other compositions were attempted, but they all produced a mixture of cubic and tetragonal phases. A third sample was created by annealing an Mg 1.1 sample, hereafter referred to as Mg 1.1A. Even if these

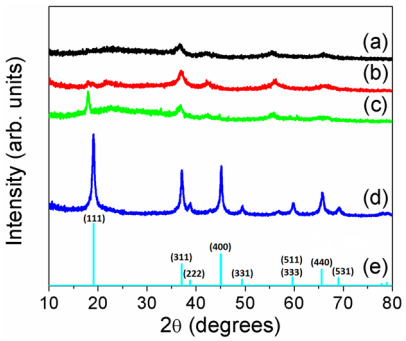

Figure 4. XRD patterns of the four $MgMn_2O_4$ samples with varying degrees of cation disorder after multiple acid treatments and full Mg removal: (a) Mg 1200, (b) Mg 1000, (c) Mg 1200A, and (d) Mg 1000A. A reference pattern for λ-MnO_2 is given in (e).

samples are perfectly ordered, some (x amount) Mg^{2+} ions are located on the octahedral sites. As they are replacing Mn^{3+} ions, they also create a corresponding number of Mn^{4+} ions, which is what causes the increased Mn oxidation state. The XRD patterns of the three starting materials and a reference pattern of a cubic Mg spinel are shown in Figure 5. The Mg 1.1 sample

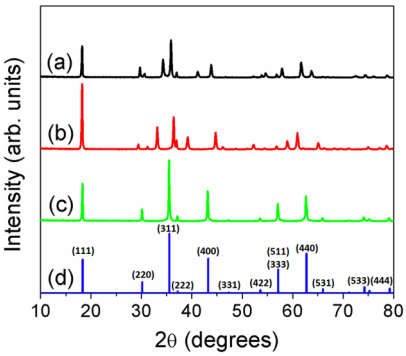

Figure 5. XRD patterns of the starting materials of the three samples in the $Mg_{1+x}Mn_{2-x}O_4$ series: (a) Mg 1.1, (b) Mg 1.1A, and (c) Mg 1.5. A reference pattern for a cubic Mg spinel is shown in (d).

is a single-phase tetragonal spinel, and the Mg 1.1A sample shows the expected significant peak shift due to changes in the cation disorder. The pattern for Mg 1.5 is surprising, however. As mentioned above, the average Mn oxidation state in Mg 1.5 is 3.33+. This compound is expected to be a tetragonal spinel because the average Mn oxidation state is below 3.5+, but this is not the case, as Mg 1.5 forms a cubic spinel. This is due to the cation disorder in the sample. It was previously stated that, when Mn^{3+} ions migrate to 8a tetrahedral sites, they are reduced to Mn^{2+} ions and oxidize a corresponding amount of Mn^{3+} ions to Mn^{4+} in the 16d octahedral sites. If this process occurs enough, the average oxidation state of the Mn ions in the octahedral sites will reach above 3.5+, causing the structure to convert to a cubic spinel. While the average Mn oxidation state of the entire structure is still 3.33+, the Mn ions in the 16d octahedral sites have an average oxidation state of >3.5+, which is what actually determines the tetragonal vs cubic phase formation.

Because raising the Mn oxidation state limits the extraction of Mg by the acid treatment mechanism, these samples are not expected to experience full Mg extraction. Table 1 details the expected final composition of the material left behind after acid

DOI: 10.1021/acsami.5b06179
ACS Appl. Mater. Interfaces 2015, 7, 22953−22961

treatment, which shows that significant Mg should remain in the structures after acid treatment. Reactions 3 and 4 convey the expected mechanism of Mg extraction in these two compounds:

$$Mg_{1.1}Mn_{1.9}^{3.05+}O_4 \rightarrow 0.55Mg_{0.36}Mn_{1.82}^{4+}O_4 + 0.9MnO + 0.9MgO \quad (3)$$

$$Mg_{1.5}Mn_{1.5}^{3.33+}O_4 \rightarrow 0.75Mg_{1.33}Mn_{1.33}^{4+}O_4 + 0.5MnO + 0.5MgO \quad (4)$$

Table 1 shows, however, that, after a single acid treatment, all three samples, especially Mg 1.1A and Mg 1.5, have substantially less Mg than expected if only Hunter's mechanism is occurring. It also shows that, as expected, Mg 1.1A had a much higher rate of Mg extraction than Mg 1.1. To see if Mg could be fully extracted from these samples, additional acid treatments were performed on Mg 1.1 and Mg 1.5. It was deemed that Mg was fully extracted from Mg 1.1A after a single treatment. Mg 1.1 required an additional two acid treatments, while Mg 1.5 required an additional four treatments. Mg 1.1 experienced full Mg extraction, and Mg 1.5 nearly did, but the amount of remaining Mg 1.5 sample was too low to do further acid treatments. The final compositions can be seen in Table 1, and their final XRD patterns can be seen in Figure 6. The XRD

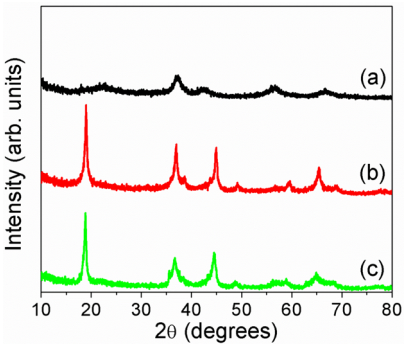

Figure 6. XRD patterns of the three samples in the $Mg_{1+x}Mn_{2-x}O_4$ series with full Mg removal: (a) Mg 1.1, (b) Mg 1.1A, and (c) Mg 1.5.

data show the same behavior as seen in the $MgMn_2O_4$ samples. Mg 1.1A produces a much more crystalline sample after acid treatment due to the increased cation order in its starting material. The acid-treated Mg 1.5 is still relatively crystalline because there is minimal cation disorder due to the increased ratio of Mg to Mn ions. Mg ions are more likely to reside in the tetrahedral sites, so increasing their population impedes Mn migration to the tetrahedral sites.

Because there was so much Mg removal beyond the anticipated amount, some other Mg extraction mechanism must be taking place in the $Mg_{1+x}Mn_{2-x}O_4$ samples. As Feng et al. previously found, Mg^{2+} ions in the octahedral sites of the spinel structure can undergo ion exchange with H^+ ions.[45] It is assumed that the same mechanism is occurring in the Mg spinel structure as well. To confirm the ion exchange of Mg^{2+} by H^+, FTIR analysis of some representative samples was taken and can be seen in Figure 7. The peaks in the 400−800 cm^{-1} range are from the Mg−O and Mn−O stretching vibrations. The peaks in the 1500−1700 cm^{-1} range correspond to the adsorbed water bending vibrations. The asymmetric stretching of carbon dioxide and water account for the peaks at ∼2400

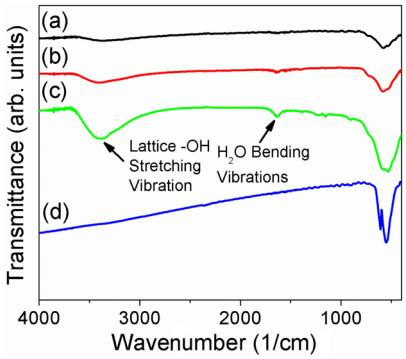

Figure 7. FTIR spectra of Mg and Li spinel samples: (a) Mg 1000, (b) Mg 1.1, (c) Mg 1.5, and (d) $LiMn_2O_4$.

and 3600−4000 cm^{-1}, respectively. This leaves the large band centered around ∼3400 cm^{-1}, which corresponds to the lattice −OH group stretching vibration.[45] When the ion-exchange reaction occurs, lattice −OH groups are formed. As the amount of Mg^{2+} ions in the octahedral sites increases from the Mg 1000 to Mg 1.1 to Mg 1.5 samples, the intensity of this band increases, signaling an increase in the degree of ion-exchange reaction. For a reference, the scan of $LiMn_2O_4$ is also included. No Li^+/H^+ ion exchange occurs in this compound, so there is no band near 3400 cm^{-1}.

This additional Mg extraction mechanism can further our understanding of several observations seen in this study. As previously described, cation disorder in these materials consists of Mg ions moving to octahedral sites in place of Mn ions, so samples with increased cation disorder have larger amounts of octahedral Mg^{2+} ions. Therefore, Mg extraction from the disordered $MgMn_2O_4$ samples probably proceeded via Hunter's mechanism and the ion-exchange reaction, even though Mn^{3+} disproportionation alone would have been able to fully extract Mg. Looking back at the $MgMn_2O_4$ data also shows that increasing the cation disorder slows the rate of Mg extraction. Because these more disordered samples experienced more of the ion-exchange reaction, it can be assumed that the ion-exchange reaction proceeds at a slower rate than the Mn disproportionation mechanism. The ion-exchange mechanism also explains why some experimental results conflicted with the ion size discussion with $MgMn_2O_4$. The slower ion-exchange reaction has a much more detrimental effect on the rate of Mg extraction than the rate increase that might be caused by the presence of smaller Mn^{4+} ions in more disordered samples.

3.3. Acid Treatment of $MgMnAlO_4$. In order to further test if $MgMn_2O_4$-based spinels follow Hunter's mechanism during acid treatment, samples were synthesized by substituting an ion besides Mg for Mn in the octahedral site. The first dopant chosen was Al because it easily forms the spinel structure with Mg in the tetrahedral sites, and a couple of compositions in the $MgMn_{2-x}Al_xO_4$ series are known. The Al^{3+} ion is substituted directly for Mn^{3+}, so there is no change to the Mn oxidation state. Unfortunately, we were only able to synthesize $MgMnAlO_4$ as a single-phase material. As discussed previously, $MgMn_2O_4$ forms in the tetragonal spinel structure, whereas $MgAl_2O_4$ adopts a cubic spinel structure. Our attempts to make other compositions in the series all produced mixtures of cubic Al-rich spinels and tetragonal Mn-rich spinels. A more thorough investigation of the phase diagram of this system could most likely produce other single-phase materials, but that was deemed outside the scope of this investigation.

DOI: 10.1021/acsami.5b06179
ACS Appl. Mater. Interfaces 2015, 7, 22953−22961

The XRD patterns of $MgMnAlO_4$ before and after acid treatment are shown in Figure 8, and it is clear that the patterns

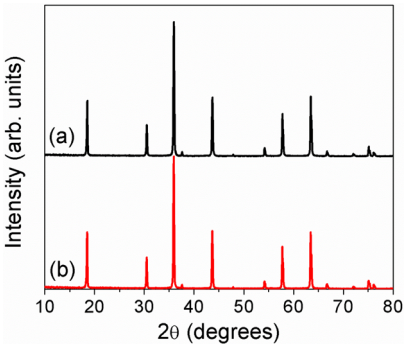

Figure 8. XRD patterns of $MgMnAlO_4$: (a) starting material and (b) after acid treatment.

are nearly identical, except for a slight peak intensity increase seen for the acid-treated sample. This is unexpected, as significant amounts of Mg should be removed, causing a lattice parameter decrease and corresponding peak shift to higher 2θ values. The XRD data depict a material unaltered by the acid treatment, which is also exactly what the ICP results confirm. The $MgMnAlO_4$ lost only 1% of its Mg during acid treatment. One possible explanation for this curious outcome is that there is so much Al^{3+} substitution in the 16d octahedral sites, that it impedes the Mn−Mn interaction/contact. As mentioned earlier in the text, the acid-treatment mechanism begins with 2 Mn^{3+} ions located next to each other disproportionating into a Mn^{2+} ion and a Mn^{4+} ion. The large population of Al^{3+} ions significantly reduces the likelihood of two Mn^{3+} ions being next to each other in the spinel structure, thus preventing the Mn^{3+} disproportionation mechanism. This explanation is contradicted, however, by our previous study on the acid delithiation of $LiMn_2O_4$-based samples.[31] In the $LiMn_{2-x}Cr_xO_4$ series, for example, Hunter's mechanism was followed for x = 0, 0.25, 0.5, 0.75, and 1. For the x = 1 sample, no Li was extracted. This is the same behavior seen in $MgMnAlO_4$, but in $LiMnCrO_4$, this is expected because all Mn ions exist in the 4+ state. In the x = 0.75 sample in $LiMn_{2-x}Cr_xO_4$, however, the mechanism is followed perfectly, as ∼20% of the Li is removed. If the Cr ions impede the Mn disproportionation process, one would expect it to have some effect on the x = 0.75 sample, but that is not the case.

This discrepancy between the Mg and Li spinels may be due to the nature of the dopant ion chosen. All of the dopant ions chosen in our previous study of $LiMn_{2-x}M_xO_4$ (M = Ni, Co, Cr, and Fe) are 3d transition-metal ions that can exist in multiple oxidation states. These transition-metal dopant ions, while impeding the formation of neighboring Mn^{3+} ions, still facilitate Mn^{3+} disproportionation by participating in the electron hopping/transfer across the shared octahedral edges in $LiMn_{2-x}M_xO_4$. Conversely, Al^{3+} is only capable of existing in the 3+ state in $MgMnAlO_4$, so it cannot facilitate such electron hopping/transfer. In order to test this theory, significant attempts were made at substituting Mn in $MgMn_2O_4$ with other transition metals, such as Co and Ni, that would still facilitate electron hopping/transfer across the shared octahedral edges. Different compositions and heating protocols were attempted, but unfortunately, none of these attempts were successful. Again, a more in-depth synthesis and structural study of these compounds would surely produce a suitable material.

3.4. Chemical Treatment of Mg Spinels. Chemical treatment with NO_2BF_4 was also used to try to extract Mg from Mg spinels. NO_2BF_4 has been used extensively to study the delithiation of Li-ion battery cathodes, such as layered oxides and spinels.[46−48] Unlike acid treatment, this chemical treatment closely mirrors the oxidative processes that occur inside electrochemical cells. For instance, stirring $LiCoO_2$ with an acetonitrile solution of NO_2BF_4 causes an extraction of Li concomitant with oxidation of Co^{3+} ions to Co^{4+} ions. In $MgMn_2O_4$, the process should follow Reaction 5 as below:

$$MgMn_2^{3+}O_4 + xNO_2BF_4 \rightarrow Mg_{1-0.5x}Mn_2^{>3+}O_4 + xNO_2 + 0.5xMg[BF_4]_2 \quad (5)$$

Also, unlike acid treatment, the degree of extraction is controlled by the amount of NO_2BF_4 added. If more NO_2BF_4 is added, then more Mg should be extracted. The mass ratio of NO_2BF_4 to active material used in this study was 4:1, which corresponds to ∼200% excess NO_2BF_4. For a comparison, a 2:1 ratio is able to fully delithiate $LiMn_2O_4$.[46]

The two samples chemically treated were $MgMn_2O_4$ and $Mg_{1.5}Mn_{1.5}O_4$, and their XRD patterns before and after the treatment with NO_2BF_4 are shown in Figure 9. It is clear that

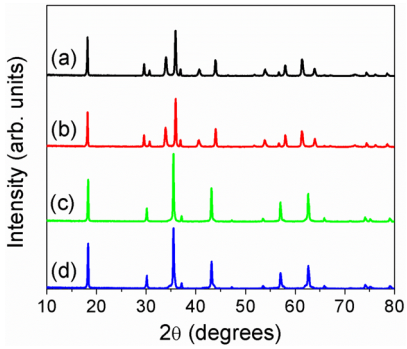

Figure 9. XRD patterns of the materials that underwent chemical treatment with NO_2BF_4 in acetonitrile medium: (a) Mg 1000 starting material, (b) Mg 1000 after chemical treatment, (c) Mg 1.5 starting material, and (d) Mg 1.5 after chemical treatment.

the chemical treatment with NO_2BF_4 essentially had no effect on the material structure as their XRD patterns are nearly identical before and after treatment. This was unexpected because removing significant amounts of Mg should decrease the lattice parameters and markedly shift the peaks to higher 2θ values. The ICP analysis, however, explains the unexpected XRD data, as both compounds showed negligible Mg removal; $MgMn_2O_4$ lost only 0.01 mol of Mg, whereas $Mg_{1.5}Mn_{1.5}O_4$ lost only 0.02 mol of Mg. This was unanticipated, especially because the same mechanism is so facile with $LiMn_2O_4$ and other Li spinels. The reason for the lack of Mg extraction may be due to the increased electrostatic repulsion that Mg^{2+} ions would feel compared to the Li^+ ions. In order to be removed from the structure, Mg ions need to diffuse from the bulk to the surface of the particle by migrating from their initial 8a tetrahedral sites to the unoccupied 16c octahedral sites and then to another 8a tetrahedral site. The electrostatic repulsion between an Mg^{2+} ion that migrated to a 16c octahedral site and an Mg^{2+} ion in a neighboring 8a tetrahedral site may be too strong to overcome,

DOI: 10.1021/acsami.5b06179
ACS Appl. Mater. Interfaces 2015, 7, 22953−22961

thus blocking the Mg^{2+} ion diffusion. The addition of Mg^{2+} and Mn^{4+} ions to the 16d octahedral sites in $Mg_{1.5}Mn_{1.5}O_4$ did not produce any Mg extraction either.

This is obviously very different behavior than was seen with the acid-treatment mechanism. Mg^{2+} ions would still have to diffuse between the 8a tetrahedral and 16c octahedral sites to be extracted during acid treatment, but the mechanism is very different in that Mn^{3+} ions are disproportionating into Mn^{2+} and Mn^{4+} ions, causing significant Mn ion migration as well as Mn ion dissolution from the lattice. The migration and dissolution of Mn ions may open up pathways with reduced electrostatic repulsion that allow the Mg^{2+} ions to diffuse through the spinel structure to be extracted. Furthermore, the two treatments involve very different solvent environments, but it is believed that this will not greatly affect the Mg^{2+} ion extraction process because the ions would not interact with the solvent until they are extracted.

These results also seem to contradict the recent work of Kim et al. that verified the intercalation of Mg^{2+} into λ-MnO_2. If they were able to electrochemically insert Mg^{2+} ions into the λ-MnO_2 structure, then one would expect to be able to remove Mg^{2+} ions from the same structural framework. One possible reason for the discrepancy is the acid treatment used in their study to prepare the λ-MnO_2 altered the morphology of some particles. Almost all of the Mg insertion occurred in particles that morphed into nanoflakes with higher surface area and shorter diffusion pathways during the acid treatment, which would enhance ion migration. The particles that did not change morphology did not show significant Mg uptake. A more important factor may be the reduced electrostatic repulsion that the migrating Mg ions would experience in the initial stages of Mg insertion into the λ-MnO_2 structure that has all of the 8a tetrahedral sites empty initially. In $MgMn_2O_4$, all of the 8a tetrahedral sites are initially filled, so any Mg^{2+} ion migrating through the 16c octahedral sites would feel the repulsion from neighboring tetrahedral Mg^{2+} ions. On the other hand, when inserting Mg^{2+} ions into the λ-MnO_2 structure, there are no Mg^{2+} ions in the 8a tetrahedral sites initially, so there is no electrostatic repulsion to block Mg migration. This would allow for Mg insertion to some degree and would explain why full Mg insertion was not achieved, because once a critical mass of Mg^{2+} ions is reached in the 8a tetrahedral sites, the diffusion may be blocked by the increased electrostatic repulsion. A final reason for their successful Mg^{2+} intercalation may be the solvating effect of water. Studies have shown that Mg^{2+} intercalation can be facilitated when water molecules provide shielding to the Mg^{2+} ions. This can be accomplished by using an aqueous electrolyte or using a material, such as birnessite, that has crystal water present in it.[11,12,49]

Combining the results from our study and other published work allows us to obtain a more complete picture of the spinel structure for use as a Mg-ion insertion host. Because NO_2BF_4 failed to extract any Mg from $MgMn_2O_4$ and $Mg_{1.5}Mn_{1.5}O_4$, it seems that the ideal spinel structure is not a viable Mg insertion/extraction host. However, structural alterations could turn the spinel structure into a usable Mg insertion host. These alterations include synthesizing particles with high surface area and decreased ion diffusion pathways,[29] chemically removing ions to reduce electrostatic repulsion,[29] or synthesizing cation-deficient spinel structures to promote Mg-ion migration.[22] The findings in this study may provide insights in designing and developing Mg-ion insertion hosts.

4. CONCLUSIONS

Battery systems using multivalent cations, such as Mg^{2+}, are being pursued as next-generation batteries, but there are several hurdles to overcome in developing Mg-ion batteries, including finding a suitable cathode that can reversibly insert/extract Mg^{2+} ions. We studied the possibility of Mg extraction in some Mg spinels, employing both acid (H_2SO_4) demagnesiation and chemical (NO_2BF_4) demagnesiation treatments analogous to those employed with lithium-containing spinels such as $LiMn_2O_4$. The samples investigated were $Mg_{1+x}Mn_{2-x}O_4$ (x = 0, 0.1, and 0.5) and $MgMnAlO_4$. It was found that acid treatment can fully extract Mg from $MgMn_2O_4$, following Hunter's mechanism[30] involving the disproportionation of Mn^{3+} and dissolution of Mn^{2+} from the lattice. The rate of Mg extraction varies linearly with the amount of cation disorder between the octahedral and tetrahedral sites, which can be altered by the heating protocol. Increasing the cation disorder decreases the rate of Mg extraction. Acid treatment can fully extract Mg from $Mg_{1.1}Mn_{1.9}O_4$ and nearly extracts all of the Mg from $Mg_{1.5}Mn_{1.5}O_4$. With only Hunter's mechanism, these compounds should have significant Mg content remaining after acid treatment, but they also experience an ion exchange of Mg^{2+} by H^+ that only happens to Mg^{2+} ions in the octahedral sites; such an ion exchange does not occur with tetrahedral sites as H^+ ions are not stable in the tetrahedral sites of the spinel lattice.[28] This mechanism is slower than the process involving Mn^{3+} disproportionation and Mn dissolution, which is why increasing cation disorder decreases the Mg extraction rate. $MgMnAlO_4$, however, does not experience Mg extraction with acid treatment because the Al^{3+} ions disrupt the Mn−Mn interaction and impede electron transfer/hopping. Chemical treatment with NO_2BF_4 was not able to extract any Mg from $MgMn_2O_4$ and $Mg_{1.5}Mn_{1.5}O_4$, unlike in the analogous $LiMn_2O_4$ spinel. This is most likely due to the increased repulsion felt by the higher valence Mg^{2+} ions by diffusing from one 8a tetrahedral site to another through the neighboring 16c octahedral sites. The difference between the acid treatment and the chemical treatment with NO_2BF_4 behaviors is due to the Mn dissolution that occurs during the acid treatment. The migration and removal of Mn ions during acid treatment lead to the Mg^{2+} ions experiencing less of an energy barrier for migration. Because the Mg^{2+} ions are not able to easily diffuse from the 8a tetrahedral sites to the neighboring 16c octahedral sites during chemical treatment with NO_2BF_4, the spinel structure may not be a suitable option for Mg-ion battery cathodes, unless it is altered structurally to increase Mg-ion migration, as shown in other reports.[22,29]

■ ASSOCIATED CONTENT

Supporting Information

The Supporting Information is available free of charge on the ACS Publications website at DOI: 10.1021/acsami.5b06179.

Detailed information on the Rietveld refinement procedure, including the methodology, calculated parameters, and plots of calculated patterns (PDF).

■ AUTHOR INFORMATION

Corresponding Author

*E-mail: rmanth@mail.utexas.edu. Phone: (512) 471-1791. Fax: (512) 471-7681.

Notes

The authors declare no competing financial interest.

DOI: 10.1021/acsami.5b06179
ACS Appl. Mater. Interfaces 2015, 7, 22953−22961

■ ACKNOWLEDGMENTS

This work was supported by the National Science Foundation Materials Interdisciplinary Research Team (MIRT) grant DMR-1122603 and the Welch Foundation grant F-1254.

■ REFERENCES

(1) Manthiram, A. Materials Challenges and Opportunities of Lithium Ion Batteries. *J. Phys. Chem. Lett.* **2011**, *2*, 176−184.
(2) Yoo, H. D.; Shterenberg, I.; Gofer, Y.; Gershinsky, G.; Pour, N.; Aurbach, D. Mg Rechargeable Batteries: An On-Going Challenge. *Energy Environ. Sci.* **2013**, *6*, 2265−2279.
(3) Lin, M. C.; Gong, M.; Lu, B.; Wu, Y.; Wang, D. Y.; Guan, M.; Angell, M.; Chen, C.; Yang, J.; Hwang, B. J.; Dai, H. An Ultrafast Rechargeable Aluminium-ion Battery. *Nature* **2015**, *520*, 324−328.
(4) Shterenberg, I.; Salama, M.; Gofer, Y.; Levi, E.; Aurbach, D. The Challenge of Developing Rechargeable Magnesium Batteries. *MRS Bull.* **2014**, *39*, 453−460.
(5) Amatucci, G. G.; Badway, F.; Singhal, A.; Beaudoin, B.; Skandan, G.; Bowmer, T.; Plitz, I.; Pereira, N.; Chapman, T.; Jaworski, R. Investigation of Yttrium and Polyvalent Ion Intercalation into Nanocrystalline Vanadium Oxide. *J. Electrochem. Soc.* **2001**, *148*, A940−A950.
(6) Chevrel, R.; Sergent, M.; Prigent, J. Sur de Nouvelles Phases Sulfurees Ternaires du Molybdene. *J. Solid State Chem.* **1971**, *3*, 515−519.
(7) Aurbach, D.; Weissman, I.; Gofer, Y.; Levi, E. Nonaqueous Magnesium Electrochemistry and its Application in Secondary Batteries. *Chem. Rec.* **2003**, *3*, 61−73.
(8) Mohtadi, R.; Matsui, M.; Arthur, T. S.; Hwang, S. J. Magnesium Borohydride: From Hydrogen Storage to Magnesium Battery. *Angew. Chem., Int. Ed.* **2012**, *51*, 9780−9783.
(9) Shao, Y.; Liu, T.; Li, G.; Gu, M.; Nie, Z.; Engelhard, M.; Xiao, J.; Lv, D.; Wang, C.; Zhang, J. G.; Liu, J. Coordination Chemistry in Magnesium Battery Electrolytes: How Ligands Affect Their Performance. *Sci. Rep.* **2013**, *3*, 3130.
(10) Zhu, J.; Guo, Y.; Yang, J.; Nuli, Y.; Zhang, F.; Wang, J.; Hirano, S.-i. Halogen-free Boron Based Electrolyte Solution for Rechargeable Magnesium Batteries. *J. Power Sources* **2014**, *248*, 690−694.
(11) Arthur, T. S.; Zhang, R.; Ling, C.; Glans, P. A.; Fan, X.; Guo, J.; Mizuno, F. Understanding the Electrochemical Mechanism of K-α-MnO_2 for Magnesium Battery Cathodes. *ACS Appl. Mater. Interfaces* **2014**, *6*, 7004−7008.
(12) Nam, K. W.; Kim, S.; Lee, S.; Salama, M.; Shterenberg, I.; Gofer, Y.; Kim, J. S.; Yang, E.; Park, C. S.; Kim, J. S.; Lee, S. S.; Chang, W. S.; Doo, S. G.; Jo, Y. N.; Jung, Y.; Aurbach, D.; Choi, J. W. The High Performance of Crystal Water Containing Manganese Birnessite Cathodes for Magnesium Batteries. *Nano Lett.* **2015**, *15*, 4071−4079.
(13) Zhang, R.; Arthur, T. S.; Ling, C.; Mizuno, F. Manganese Dioxides as Rechargeable Magnesium Battery Cathode; Synthetic Approach to Understand Magnesiation Process. *J. Power Sources* **2015**, *282*, 630−638.
(14) Novak, P.; Desilverstro, J. Electrochemical Insertion of Magnesium into Metal Oxides and Sulfides from Aprotic Electrolytes. *J. Electrochem. Soc.* **1993**, *140*, 140−144.
(15) Spahr, M. E.; Novak, P.; Haas, O.; Nesper, R. Electrochemical Insertion of Lithium, Sodium, and Magnesium in Molybdenum(IV) Oxide. *J. Power Sources* **1995**, *54*, 346−351.
(16) Feng, Z.; Yang, J.; NuLi, Y.; Wang, J. Sol−gel Synthesis of $Mg_{1.03}Mn_{0.97}SiO_4$ and its Electrochemical Intercalation Behavior. *J. Power Sources* **2008**, *184*, 604−609.
(17) Zheng, Y.; NuLi, Y.; Chen, Q.; Wang, Y.; Yang, J.; Wang, J. Magnesium Cobalt Silicate Materials for Reversible Magnesium Ion Storage. *Electrochim. Acta* **2012**, *66*, 75−81.
(18) Giraudet, J.; Claves, D.; Guérin, K.; Dubois, M.; Houdayer, A.; Masin, F.; Hamwi, A. Magnesium Batteries: Towards a First Use of Graphite Fluorides. *J. Power Sources* **2007**, *173*, 592−598.
(19) Vatsala Rani, J.; Bhavana Rushi, S.; Kanakaiah, V.; Palaniappan, S. Green Fluorination of Natural Graphite and its Application in Rechargeable Magnesium Ion Transfer Battery. *J. Electrochem. Soc.* **2011**, *158*, A1031−A1035.
(20) Novak, P.; Sheifele, W.; Joho, F.; Haas, O. Electrochemical Insertion of Magnesium into Hydrated Vanadium Bronzes. *J. Electrochem. Soc.* **1995**, *142*, 2544−2550.
(21) Novak, P.; Scheifele, W.; Haas, O. Magnesium Insertion Batteries - An Alternative to Lithium? *J. Power Sources* **1995**, *54*, 479−482.
(22) Sanchez, L.; Pereira-Ramos, J.-P. Electrochemical Insertion of Magnesium in a Mixed Manganese-Cobalt Oxide. *J. Mater. Chem.* **1997**, *7*, 471−473.
(23) Makino, K.; Katayama, Y.; Miura, T.; Kishi, T. Electrochemical Insertion of Magnesium to $Mg_{0.5}Ti_2(PO_4)_3$. *J. Power Sources* **2001**, *99*, 66−69.
(24) Makino, K.; Katayama, Y.; Miura, T.; Kishi, T. Preparation and Electrochemical Magnesium Insertion Behaviors of $Mg_{0.5+y}(Me_yTi_{1-y})_2(PO_4)_3$ (Me = Cr, Fe). *J. Power Sources* **2002**, *112*, 85−89.
(25) Gregory, T. D.; Hoffman, R. J.; Winterton, R. C. Nonaqueous Electrochemistry of Magnesium: Applications to Energy Storage. *J. Electrochem. Soc.* **1990**, *137*, 775−780.
(26) Ling, C.; Mizuno, F. Phase Stability of Post-spinel Compound AMn_2O_4(A = Li, Na, or Mg) and Its Application as a Rechargeable Battery Cathode. *Chem. Mater.* **2013**, *25*, 3062−3071.
(27) Yuan, C.; Zhang, Y.; Pan, Y.; Liu, X.; Wang, G.; Cao, D. Investigation of the Intercalation of Polyvalent Cations (Mg^{2+}, Zn^{2+}) into λ-MnO_2 for Rechargeable Aqueous Battery. *Electrochim. Acta* **2014**, *116*, 404−412.
(28) Sinha, N. N.; Munichandraiah, N. Electrochemical Conversion of $LiMn_2O_4$ to $MgMn_2O_4$ in Aqueous Electrolytes. *Electrochem. Solid-State Lett.* **2008**, *11*, F23−F26.
(29) Kim, C.; Phillips, P. J.; Key, B.; Yi, T.; Nordlund, D.; Yu, Y. S.; Bayliss, R. D.; Han, S. D.; He, M.; Zhang, Z.; Burrell, A. K.; Klie, R. F.; Cabana, J. Direct Observation of Reversible Magnesium Ion Intercalation into a Spinel Oxide Host. *Adv. Mater. (Weinheim, Ger.)* **2015**, *27*, 3377−3384.
(30) Hunter, J. C. Preparation of a New Crystal Form of Manganese Dioxide: λ-MnO_2. *J. Solid State Chem.* **1981**, *39*, 142−147.
(31) Knight, J. C.; Therese, S.; Manthiram, A. Delithiation Mechanisms in Acid of Spinel $LiMn_{2-x}M_xO_4$ (M = Cr, Fe, Co, and Ni) Cathodes. *J. Electrochem. Soc.* **2015**, *162*, A426−A431.
(32) Manaila, R. Cation Migration in Tetragonal Spinels ($MgMn_2O_4$). *J. Phys. Chem. Solids* **1967**, *28*, 2335−2341.
(33) Romeijn, F. C. Physical and Crystallographical Properties of Some Spinels. *Philips Res. Rep.* **1953**, *8*, 304−320.
(34) Sinha, A. P. B.; Sanjana, N. R.; Biswas, A. B. On the Structure of Some Manganites. *Acta Crystallogr.* **1957**, *10*, 439−440.
(35) Irani, K. S.; Sinha, A. P. B.; Biswas, A. B. Effect of Temperature on the Structure of Manganites. *J. Phys. Chem. Solids* **1962**, *23*, 711−727.
(36) Kshirsagar, S. T.; Biswas, A. B. Crystallographic Studies of Some Mixed Manganite Spinels. *J. Phys. Chem. Solids* **1967**, *28*, 1493−1499.
(37) Rosenberg, M.; Nicolau, P. Electrical Properties and Cation Migration in $MgMn_2O_4$. *Phys. Status Solidi B* **1964**, *6*, 101−110.
(38) Manaila, R.; Pausescu, P. Structural Changes in $MgMn_2O_4$ at High Temperatures. *Phys. Status Solidi B* **1965**, *9*, 385−394.
(39) Radhakrishnan, N. K.; Biswas, A. B. A Neutron Diffraction Study of the Cation Migration in $MgMn_2O_4$. *Phys. Status Solidi A* **1976**, *37*, 719−722.
(40) Barkhatov, V. P.; Balakirev, V. F.; Golikov, Y. V.; Kostitsin, E. G. X-Ray Diffraction Investigation of Cation Distribution in High-Temperature Cubic Spinels of Mg-Mn-O System. *Phys. Status Solidi A* **1983**, *76*, 57−63.
(41) Azzoni, C. B.; Mozzati, M. C.; Malavasi, L.; Ghigna, P.; Flor, G. Magnetic and X-ray Diffraction Investigation on $Mg_{1-x}Mn_{2+x}O_4$ Spinels. *Solid State Commun.* **2001**, *119*, 591−595.
(42) Malavasi, L.; Ghigna, P.; Chiodelli, G.; Maggi, G.; Flor, G. Structural and Transport Properties of $Mg_{1-x}Mn_xMn_2O_{4\pm\delta}$ Spinels. *J. Solid State Chem.* **2002**, *166*, 171−176.

DOI: 10.1021/acsami.5b06179
ACS Appl. Mater. Interfaces 2015, 7, 22953−22961

(43) Malavasi, L.; Tealdi, C.; Flor, G.; Amboage, M. High-Pressure Stability of the Tetragonal Spinel $MgMn_2O_4$: Role of Inversion. *Phys. Rev. B: Condens. Matter Mater. Phys.* **2005**, *71*, 174102.
(44) Panda, S. K.; Jung, I.-H.; Bessmann, T. Critical Evaluation and Thermodynamic Modeling of the Mg-Mn-O (MgO-MnO-MnO_2) System. *J. Am. Ceram. Soc.* **2014**, *97*, 3328−3340.
(45) Feng, Q.; Miyai, Y.; Kanoh, H.; Ooi, K. Li^+ and Mg^{2+} Extraction and Li^+ Insertion Reactions with $LiMg_{0.5}Mn_{1.5}O_4$ Spinel in the Aqueous Phase. *Chem. Mater.* **1993**, *5*, 311−316.
(46) Chebiam, R. V.; Kannan, A. M.; Prado, F.; Manthiram, A. Comparison of the Chemical Stability of the High Energy Density Cathodes of Lithium-ion Batteries. *Electrochem. Commun.* **2001**, *3*, 624−627.
(47) Chebiam, R. V.; Prado, F.; Manthiram, A. Comparison of the Chemical Stability of $Li_{1-x}CoO_2$ and $Li_{1-x}Ni_{0.85}Co_{0.15}O_2$ Cathodes. *J. Solid State Chem.* **2002**, *163*, 5−9.
(48) Choi, J.; Alvarez, E.; Arunkumar, T. A.; Manthiram, A. Proton Insertion into Oxide Cathodes During Chemical Delithiation. *Electrochem. Solid-State Lett.* **2006**, *9*, A241−A244.
(49) Novak, P.; Imhof, R.; Haas, O. Magnesium Insertion Electrodes for Rechargeable Nonaqueous Batteries - A Competitive Alternative to Lithium? *Electrochim. Acta* **1999**, *45*, 351−367.

DOI: 10.1021/acsami.5b06179
ACS Appl. Mater. Interfaces 2015, 7, 22953−22961